M&C 2017 - International Conference on Mathematics & Computational Methods Applied to Nuclear Science & Engineering, Jeju, Korea, April 16-20, 2017, on USB (2017)

Practical Resolution of Angle Dependency of Multigroup Resonance Cross Sections Using Parametrized Spectral SPH Factors

Hansol Park and Han Gyu Joo*

Seoul National University, 1 Gwanak-ro, Gwanak-gu, Seoul, 151-744, Korea
** joohan@snu.ac.kr*

Abstract – *Based on the observation that the ignorance of the angle dependency of multigroup resonance cross sections within a fuel pellet would result in nontrivial underestimation of the spatial self-shielding of flux, namely the overestimation of flux itself inside the pellet, a parametrized spectral super homogenization (SPH) factor library method is developed as a practical means of resolving the problem. Region-wise spectral SPH factors are calculated by the normal and transport corrected SPH iterations after performing ultra-fine group slowing down calculation over various light water reactor pin-cell configurations. The parametrization is done with fuel temperature, U238 number density, fuel radius, moderator source represented by $\Sigma_{mod}V_{mod}$, and the number density ratio of resonance nuclides to that of U238 in a form of resonance interference correction factors. The parametrization turns out to be successful in that the root mean square errors of the interpolated SPH factors over the fuel regions of various pin-cells are within 0.1% RMS. The improvement in reactivity error of the proposed method is shown to be superior to that by the old SPH method in that the reactivity bias of about -200 to -300 caused by the overestimation of the resonance group flux vanishes almost completely for most cases. It is demonstrated that the proposed method is effective in the assembly problems as well despite that the SPH factors are generated from pin cell calculations. In this regard, it is conformed that considering only the local effect is sufficient because the surrounding effect takes only about 4% in the reactivity improvement.*

I. INTRODUCTION

Proper treatment of resonance self-shielding has been of great importance in multigroup (MG) core calculations. A lot of effort has been made to generate accurate resonance MG cross sections (XSs). However, we note that the current resonance treatment focusing on MG XSs is not sufficient because the corresponding MG flux cannot be accurate if the angle dependency of resonance MG XSs is not properly incorporated. Since the reaction rate cannot be right if there is an error in the resonance flux, nontrivial biases as large as -300 pcm are introduced in the reactivity of the pin cell and assembly problems as demonstrated later in this paper. Thus the angle dependency of resonance MG XSs should be properly addressed for rigorous resonance treatment. The angle dependency of the XS in the MG transport equation was recognized long ago and a partial incorporation of the angle dependency in terms of transport correction was suggested. [1] However, it turned out in our earlier trials that this method is not effective in dealing with significant angle dependency in the cases of resonance MG XSs.

The angle dependency problem of resonance MG XS was also noted in a quite recent work by Gibson [2] in which the use of spectral super homogenization (SPH) factors [3] was suggested as one of the candidates for the resolution of angle dependency. However, no specific generalization of the usage of the SPH factors was provided. In fact, the spectral SPH factor was introduced first by Hebert [4] to force the conservation of reaction rates in the process of subgroup to group condensing, but there was no mention about its connection to the ignorance of the angle dependency of resonance MG XSs. The term *spectral* is attached here to distinguish the SPH factor for energy condensation from that for *spatial* homogenization.

In the work here, the problem of neglecting the angle dependency of resonance MG XSs is first investigated thoroughly and a method for generalizing the usage of the spectral SPH factors is introduced by parametrizing them over various pin-cell characterization parameters such as geometry, composition and the relative abundance of fuel to moderator. The issues on the actual implementation of the new method, such as how to apply it to the cases with an arbitrary number of subrings in a pellet and to the cases with different scattering anisotropy treatments, will also be discussed. In the verification section, the significance of the proposed method will be discussed in detail by analyzing the changes in the resultant spectrum for various pin-cells and the improvement in the group-wise component of reactivity error. Lastly, the effect of the surrounding environment will be quantified through assembly test cases.

II. ANGLE DEPENDENCY OF RESONANCE MG XS

In order to figure out how much resonance MG XSs depend on neutron angle, angular flux spectra were computed by a method of characteristics (MOC) based in-house ultra-fine group slowing down code EXUS for a pin cell problem shown in Fig. 1. The resulting angular flux distribution for the fine energy points within a group containing the 6.67 eV resonance of U-238 - the 19th group

(G19) in our MG library group structure - are shown on the left of Fig. 2. Each closed curve here represents azimuthal distribution of angular flux for the polar angle closest to the x-y plane at Region 15 for each energy point in the 19th group. Because of the difference in self-shielding for the incoming neutron rays and outgoing rays of the fuel, the effective XS becomes very much dependent on angle as shown on the right of Fig. 2. In spite of this big difference, however, the total XS weighted by the scalar flux spectrum is being used in almost all MG transport solvers.

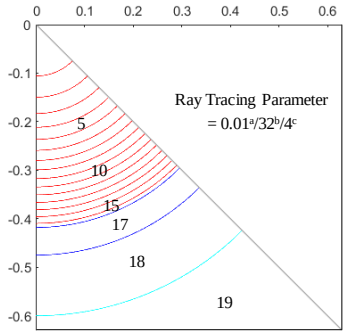

Region #	Region Name
1-15	Fuel (UO2)
16	Gap
17	Cladding
18-19	Moderator

a) Ray spacing
b) # of azimuthal angles in $\frac{\pi}{2}$
c) # of polar angles in upper hemisphere

Fig. 1. Geometry, composition and ray-tracing parameters for the ultra-fine group calculation.

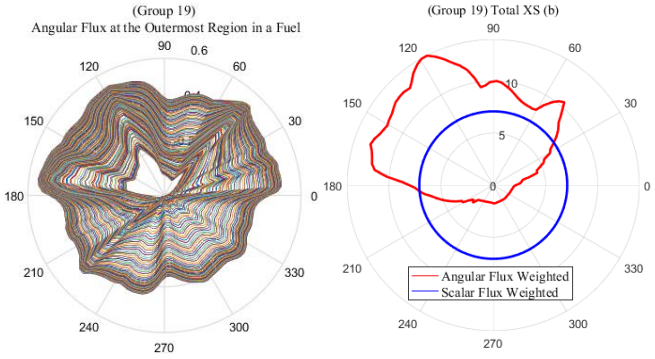

Fig. 2. (Left) Azimuthal distribution of angular fluxes for a polar angle at Region 15 at every energy point in G19/ (Right) Effective total XS weighted by angular flux spectra and scalar flux spectrum for G19.

This large discrepancy between the angle-dependent MG XSs and the constant one, in turn, makes the incoming current over-estimated because smaller XS is used instead of the large XS for the incoming neutrons. The opposite is true for the outgoing neutrons. This leads to a distorted angular flux shape which is more skewed toward the fuel as shown by the blue line on the left plot of Fig. 3.

For a given scattering source to the fuel, larger current into the fuel makes intra-pellet flux level higher as shown in Fig. 4. The group flux calculated by the nTRACER direct whole core calculation code [5] was largely over-estimated in the fuel compared to the flux of the McCARD Monte Carlo code [6] even though the reference MG XSs generated by McCARD were used. On the contrary, the condensed flux obtained from the ultra-fine group slowing down solution, the EXUS result, matched well with the McCARD flux shape.

The resulting groupwise reactivity errors due to higher absorption and nu-fission rates are shown in Table I for major resonance groups. McCARD generated MG XSs for all the regions were used in the nTRACER calculation so that the error should be considered to be solely due to the flux error caused by the ignorance of the angle dependency of resonance MG XSs.

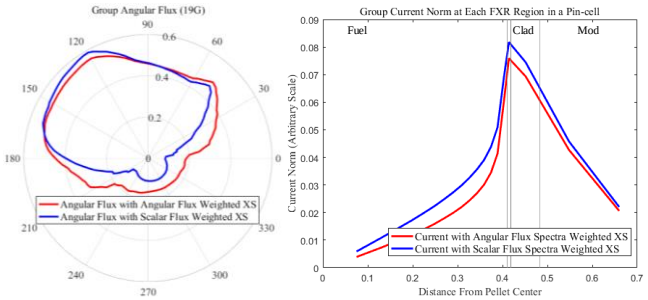

Fig. 3. (Left) Comparison of the group angular fluxes for a polar angle calculated by using angular flux spectra weighted and scalar flux spectrum weighted total XSs at Region 15 in G19/ (Right) Comparison of the corresponding group current norms at all regions across the pin-cell in G19.

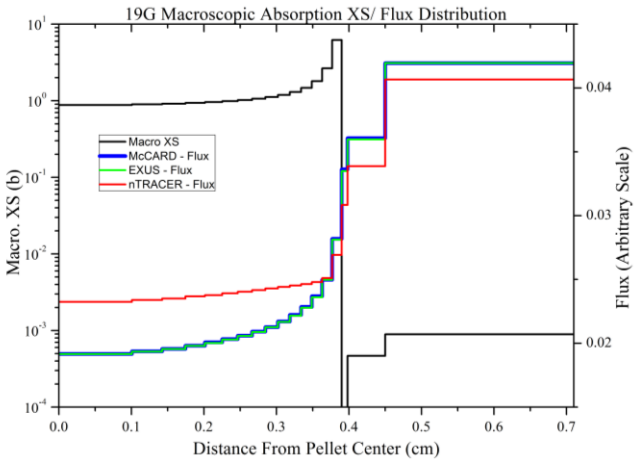

Fig. 4. Under-estimation of spatial self-shielding of flux by nTRACER leading to over-estimation of flux inside the fuel

Table I. Group-wise reactivity error (pcm) due to flux over-estimation (Reference k-eff = 1.33467)

Reaction	11G	12G	13G	14G	15G	19G
Abs.	-46	-28	-14	-43	-41	-130
NuFis.	+30	+15	+16	+29	+31	+12
Net	-16	-13	+2	-14	-10	-118

This phenomenon occurs commonly for arbitrary group structures as shown in Fig. 5 where the relative errors of fuel averaged flux in the resonance groups for four different group structures are displayed. This leads to larger resonance absorption and nu-fission rates in the pellet, and

end up with having very large net negative reactivity error of about -200 to -300 pcm for all the group structures because the influence of resonance absorption to the net reactivity is larger than that of resonance nu-fission. Note that all the following test results to be presented in this paper were generated using the 47G structure noting that the irrelevance of the group structure.

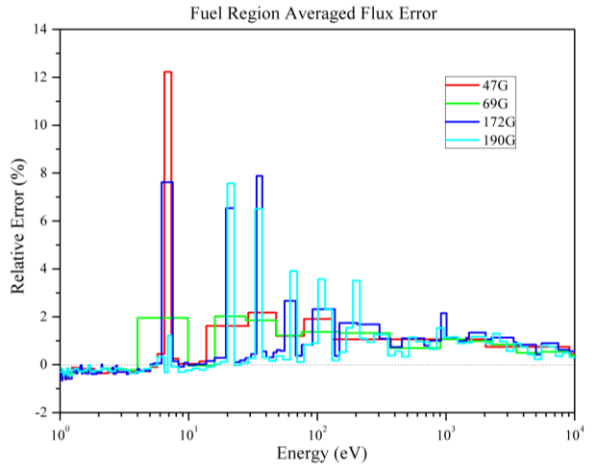

Fig. 5. Relative errors of fuel averaged flux of nTRACER to that of McCARD in resonance groups for various group structures: 47G, 69G, 172G and 190G

Table II. Reactivity errors for various group structures (Reference k-eff = 1.33467)

Group Structure	K-eff	Δρ (pcm)	From resonance groups	
			Absorption	Nu-Fission
47G	1.32998	-264	-314	+76
69G	1.33141	-183	-239	+85
172G	1.32799	-377	-430	+83
190G	1.33040	-240	-269	+51

III. RESOLUTION WITH SPECTRAL SPH FACTOR

As the practical means of the angle dependency of the resonance MG XS, the spectral SPH is considered in this work. In the original paper by Hebert [4], spectral SPH factors were defined over isotopes in order to alleviate the reaction rate error in the subgroup to group condensing process. Also, the SPH corrected XSs were defined for all reaction types and they were assumed to be the final products from the resonance treatment. In the work here, however, the SPH factors are not used in the resonance treatment step, but in the transport calculation phase. The details of this new approach and the associated generation and parameterization procedures are given below.

1. New Interpretation of Spectral SPH Factors

Consider the following reference transport operator containing the angle dependent XS and the typical one neglecting the angle dependency:

$$\boldsymbol{T}_g = \Omega\cdot\nabla + \Sigma_g(r,\Omega) \tag{1}$$

and

$$\boldsymbol{T}_g = \Omega\cdot\nabla + \Sigma_g(r)\,. \tag{2}$$

After finishing the resonance calculation, the SPH factor is introduced as an intermediate parameter which forces the typical transport operator of Eq. (2) to yield the reference reaction rate in the non-moderator region of the true operator of Eq. (1) by modifying the operator from Eq. (2) to Eq. (3) below through the use of the position dependent SPH factor, $\mu_g(r)$:

$$\boldsymbol{T}_{g,\mu_g} = \Omega\cdot\nabla + \mu_g(r)\Sigma_g(r)\,. \tag{3}$$

Here $\mu_g(r)$ is a free parameter that can be determined by the following constraint:

$$\int_{V_{Non-Mod}} d^3r\int_\Omega d\Omega \boldsymbol{T}^{col}_{g,\mu_g}\tilde{\psi}_{g,\mu_g}(r,\Omega) = \int_{V_{Non-Mod}} d^3r\int_\Omega d\Omega \boldsymbol{T}^{col}_{g}\psi_{g}(r,\Omega) \tag{4}$$

where the superscript *col* means the collision part of the operator. Since the same reference scattering source in the non-moderator region is to be used in both SPH corrected and uncorrected balance equations, Eq. (4) would force the total leakage of the pellet resulting from the streaming operator of Eq. (3) to be the same as that of Eq. (1).

Eq. (4) can be rewritten as follows:

$$\begin{aligned}\int_{V_{Non-Mod}} d^3r\int_\Omega d\Omega\mu_g(r)\Sigma_g(r)\tilde{\psi}_{g,\mu_g}(r,\Omega)\\ = \int_{V_{Non-Mod}} d^3r\int_\Omega d\Omega\Sigma_g(r,\Omega)\psi_g(r,\Omega)\end{aligned} \tag{5}$$

or in terms of scalar flux as:

$$\int_{V_{Non-Mod}} d^3r\mu_g(r)\Sigma_g(r)\tilde{\phi}_{g,\mu_g}(r) = \int_{V_{Non-Mod}} d^3r\Sigma_g(r)\phi_g(r)\,. \tag{6}$$

Eq. (6) suggests two possible ways to determine $\mu_g(r)$: the first to match the total reaction rate in the entire non-moderator region and the second to match region-wise reaction rates. In this paper, the latter is taken since the former is not desirable in a depletion calculation where the intra-pellet burnup profile is important. Fig. 6 demonstrates that the use of the average SPH factor defined by the following

$$\mu_g = \frac{\int_{V_{Non-Mod}} d^3r\Sigma_g(r)\phi_g(r)}{\int_{V_{Non-Mod}} d^3r\Sigma_g(r)\tilde{\phi}_{g,\mu_g}(r)} \tag{7}$$

makes the intra-pellet flux distribution far much different from the reference one even though the total reaction rate is preserved.

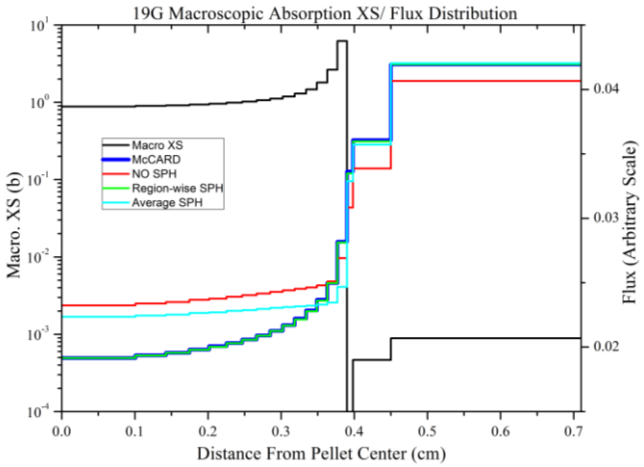

Fig. 6. Improperness of intra-pellet flux distribution with the use of fuel region averaged SPH factor

By this reason, the spectral SPH factor should be determined region-wise simply as Eq. (8) for each region *r* taking the advantage of uniform XS within the region:

$$\mu_g^r = \frac{\phi_g^r}{\tilde{\phi}_{g,\mu_g}^r} . \tag{8}$$

The spectral SPH factors defined above can be in the MOC calculation as follows:

Determine the total XSs of all regions using the ultrafine group slowing solution.

In the MOC sweep for each resonance group, modify the transport operator from Eq. (2) to Eq. (3) by multiplying region-wise $\mu_g(r)$ to $\Sigma_g(r)$ just before the ray tracing.

Perform the ray-tracing to obtain the scalar fluxes.

Right after the ray-tracing, multiply the same $\mu_g(r)$ to the ray-tracing solution, $\tilde{\phi}_{g,\mu_g}(r)$, to obtain the true solution, $\phi_g(r)$.

2. Determination of Spectral SPH Factor

The pre-generation of spectral SPH factors consists of two steps: the ultra-fine group slowing down calculation and the SPH iteration. The detailed transport calculation at the first step should be as accurate as possible. In this work, the MOC calculation in EXUS was performed with 0.01 ray spacing, 32 azimuthal angles in a quadrant, and 4 optimum polar angle set in the upper hemisphere with 15 fuel subdivisions and 8 sectors in 2π with an ultra-fine group structure involving 800,000 groups. As for the treatment of anisotropic scattering, only P0 scattering source was considered because EXUS is not able to treat Pn scattering source in its slowing down calculation. In principle, as highest order of scattering treatment as possible is better to be used in solving slowing down calculation. It turned out, however, that the spectral SPH factor library generated by P0 slowing down scheme gave accurate enough results as shown later.

In the second step, the spectral SPH factors should be determined through an iteration procedure described below. In the following, the spatial or regional dependence of various physical quantities such as flux and cross sections is denoted by the position vector *r*. The region average quantities are to be obtained after spatial integration over the region. Note that the integration procedure is omitted for the simplicity. The spectral SPH are obtained through the following procedure

:

Obtain region-wise reference scalar flux $\phi_g(r)$, scattering source, $Q_g(r)$, and total XS, $\Sigma_g(r)$ by the following for Group g.

$$\phi_g(r) = \int_g \phi(r,E)dE , \tag{9}$$

$$Q_g(r) = \int_g Q(r,E)dE , \tag{10}$$

and

$$\Sigma_g(r) = \int_g \Sigma(r,E)\phi(r,E)dE \Big/ \int_g \phi(r,E)dE . \tag{11}$$

All the quantities on the RHS of the above equations are the products of the slowing down solver.

Solve the following with $\mu_g^{(0)}(r)=1$ at all regions to obtain $\tilde{\phi}_{g,\mu_g}^{(1)}(r)$.

$$\boldsymbol{T}_{g,\mu_g}^{(0)} \tilde{\phi}_{g,\mu_g}^{(1)}(r) = Q_g(r) \tag{12}$$

Update $\mu_g^{(1)}(r)$ as following.

$$\text{Non-Mod. Region} : \mu_g^{(1)}(r) = \frac{\phi_g(r)}{\tilde{\phi}_{g,\mu_g}^{(1)}(r)}$$
$$\text{Mod. Region} : \mu_g^{(1)}(r) = 1 \tag{13}$$

Solve the transport equation with updated operator, $\boldsymbol{T}_{g,\mu_g}^{(L)}$, to obtain $\tilde{\phi}_{g,\mu_g}^{(L+1)}(r)$, and update $\mu_g^{(L+1)}(r)$. Repeat this procedure until the following criteria holds:

$$\underset{r\in Non-Mod.}{MAX} \left\{ \frac{\left|\mu_g^{(L+1)}(r) - \mu_g^{(L)}(r)\right|}{\mu_g^{(L)}(r)} \right\} < 10^{-6} . \tag{14}$$

A. Transport Corrected SPH Iteration

In the actual nTRACER transport calculations, transport correction method is applied for P0 calculations. This introduces a discrepancy in the scattering sources and total XSs between the transport calculation and the slowing down calculation. Therefore there should be a correction in the normal SPH iteration for transport corrected P0 calculations. The way of correction depends on what kind of transport correction is applied to the library being used in the transport calculation. In our library, outflow or inflow

transport corrections are being used. Because difference between those two is small in resonance groups [7], outflow based transport correction is applied to the normal SPH iteration as follows because of its easy implementation.

The transport corrected SPH iteration procedure is the same up to the step a) with the normal SPH iteration. Before the step b), the following corrections are applied:

$$\Sigma_g(r) \to \Sigma_g(r) - \sum_{iso \in r} \int_g \Sigma_{s,1}^{iso}(r,E)\phi(r,E)dE \Big/ \phi_g(r)$$
$$Q_g(r) \to Q_g(r) - \sum_{iso \in r} \int_g \Sigma_{s,1}^{iso}(r,E)\phi(r,E)dE \Big/ \phi_g(r) . \quad (15)$$

Here, the first order scattering XS, $\Sigma_{s,1}^{iso}(r,E)$, can be obtained by Eq. (16) with the assumption that s-wave scattering approximation holds for major isotopes in LWR in resonance energy range.

$$\Sigma_{s,1}^{iso}(r,E) = \frac{2}{3A^{iso}} \Sigma_{s,0}^{iso}(r,E) \quad (16)$$

From Step b), the procedure is the same except the usage of transport corrected total XSs and scattering sources.

For the Pn calculation in a transport calculation, the spectral SPH factors should be generated by the normal SPH iteration because total XSs and scattering sources in the transport calculation are not corrected. Table III supports that transport corrected P0 calculation should use SPH factors using the transport corrected SPH iteration and higher order calculations should use SPH factors using the normal SPH iteration. In these calculations, the McCARD XSs were used at all regions in the nTRACER calculation with transport correction while the Pn scattering matrices were taken from the nTRACER library. Fig. 7 also shows large flux errors in the fuel for the P0 calculation with the normal SPH iteration and the Pn calculations with the transport corrected SPH iteration.

Table III. Scattering Treatment Test in nTRACER

SPH Iteration	Scat. Order	K-eff	Δρ (pcm)	Reso. Groups	
				Abs.	NuFis.
McCARD		1.33467	8 (S.D.)	-	-
Normal	P0	1.33521	+30	+45	-13
	P1	1.33434	-19	-38	+21
	P2	1.33471	+2	-8	+5
	P3	1.33463	-2	-13	+6
Transport Corrected	P0	1.33454	-7	0	+3
	P1	1.33368	-56	-79	+31
	P2	1.33406	-34	-48	+15
	P3	1.33398	-39	-54	+17

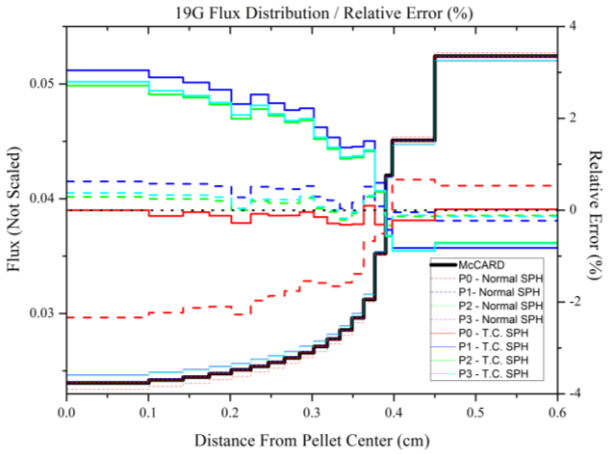

Fig. 7. G17 flux errors of P0 to P3 transport calculations for different choices of SPH factors obtained by either normal or transport corrected SPH iterations.

B. Spatial Interpolation of SPH Factor for Different Number of Subrings in a Fuel

Since region-wise spectral SPH factors are used, there should be a provision for the cases where the number of subrings in a fuel for the actual transport calculation is different from that used in the generation step. The behavior of region-wise spectral SPH factors calculated by using different number of subrings in a fuel is shown in Fig. 8. The reference slowing down calculation was done with 15 subrings, and for other cases, total XSs and scattering sources, $\Sigma_g^{k_N}$ and $Q_g^{k_N}$, used for their SPH iterations were obtained by homogenizing them as Eq. (17).

$$\Sigma_g^{k_N} = \sum_{k_{15} \in k_N} \Sigma_g^{k_{15}} \phi_g^{k_{15}} V^{k_{15}} \Big/ \sum_{k_{15} \in k_N} \phi_g^{k_{15}} V^{k_{15}}$$
$$Q_g^{k_N} = \sum_{k_{15} \in k_N} Q_g^{k_{15}} V^{k_{15}} \Big/ V^{k_N} . \quad (17)$$

where k_N is the region index of the N subrings case. In the process of homogenization, all physical quantities were assumed to be flat in a region.

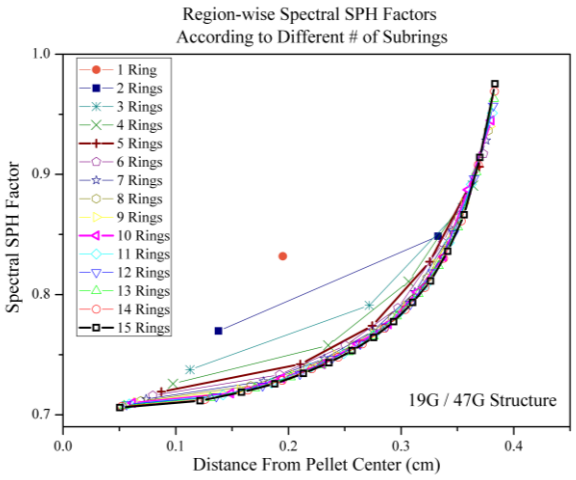

Fig. 8. Region-wise spectral SPH factors for different number of subrings in the fuel

In fact, there's no interpolation issue if spectral SPH factors for all the possible number of subrings, e.g. 1 to 15, are provided. Then, however, the file size becomes 8 times bigger and thus this is better to be avoided.

Another way would be to provide the reference XSs, fluxes and scattering sources to the transport code and to implement the SPH iteration on the fly after the homogenization for the specific pin-cell configuration. In that case, however, the file size becomes 3 times bigger and it will also require an additional time for the SPH iteration. To avoid these problems, two approximate interpolation schemes are devised and compared: a direct interpolation and a flux conversion scheme.

The direct interpolation literally means that the spectral SPH factor at the middle position of a concentric ring is linearly interpolated by using the table of the spectral SPH factor versus its middle position of a ring. However, Fig. 8 implies that the direct interpolation scheme may not work well. Considering this weakness of direct interpolation, the flux conversion scheme was devised and tested. The description is as follow.

$$\mu_g^{k_N} = \frac{\phi_g^{k_N}}{\tilde{\phi}_{g,\mu_g}^{k_N}} \tag{18}$$

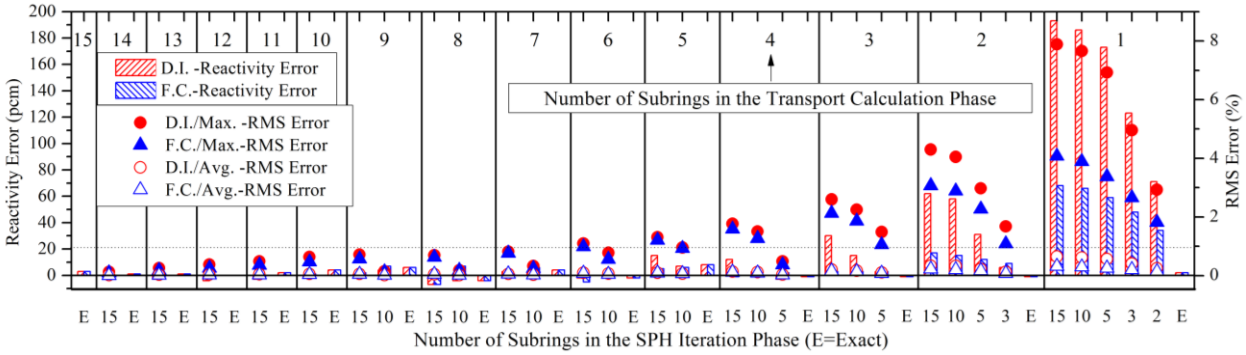

Fig. 9. Space interpolation test result (Reference K-eff : 1.33467(8))

D.I. : Direct Interpolation, F.C. : Flux Conversion, RMS Error : $\Delta\mu_g = 100\sqrt{\sum_{i=1}^{N}\left(\frac{\mu_{g,i}^{(\text{interp.})} - \mu_{g,i}^{(\text{exact})}}{\mu_{g,i}^{(\text{exact})}}\right)^2 \Big/ N}$ (N : # of subrings)

Max./Avg. : Maximum/Average value of $\Delta\mu_g$ among resonance groups

In order to obtain $\mu_g^{k_N}$ in Eq. (18), SPH corrected fluxes at N subrings in a fuel should be given. In principle, this should be calculated by SPH iteration, but it is obtained by just homogenization from those at 15 subrings in a fuel like a reference flux as in Eq. (19). This approximation goes wrong if N is smaller, but lies on better physical ground than the direct interpolation. For this, both spectral SPH factors and SPH corrected fluxes should be provided to a transport code.

$$\phi_g^{k_N} = \sum_{k_{15}\in k_N} \phi_g^{k_{15}} V^{k_{15}} \Big/ V^{k_N}, \quad \tilde{\phi}_{g,\mu_g}^{k_N} = \sum_{k_{15}\in k_N} \tilde{\phi}_{g,\mu_g}^{k_N} V^{k_{15}} \Big/ V^{k_N} \tag{19}$$

Fig. 9 compares the results of the two methods. nTRACER calculation used McCARD XSs at all regions. The x-axis for each case indicates the number of subrings in a fuel with which the exact SPH factor to be used for the interpolation is generated. Two methods give essentially the same accuracy up to 6 subrings, considering the standard deviation, and the flux conversion scheme is obviously betterfor smaller number of subrings. However, the absolute error is not negligible even with the flux conversion scheme so that additional tabulation for small number of subrings cases is needed. If so, there's no advantage to use the flux conversion scheme, since it needs twice more data than the direct interpolation. In this reason, with about 0.5% RMS error criteria, it was decided to use the direct interpolation with the tabulation of 15, 10, 5, 3, 2, 1 subrings cases instead of the flux conversion scheme. In this way, file size is less than 3 time bigger and additional time is not required without loss of accuracy.

3. Parametrization of Spectral SPH Factor

In principle, the spectral SPH factor is to be applied, it should be pre-generated at the same problem of interest unless ultra-fine group slowing down approach is adopted for the resonance treatment. To be practical and applicable to any resonance treatment, we suggest the parametrization of the spectral SPH factor.

Based on the observation that the factor behaves smoothly over the abundance of fuel (mainly U238 for LWR) and moderator as shown in Fig. 10, a parametrization strategy was devised to functionalize the factor over square root of temperature, U238 number density, fuel radius and a measure of the moderator source, $\Sigma_{mod}V_{mod.}$

The reason why the moderator dimension and density effect were combined in one parameter is shown in Fig. 10 where the same fractional changes in each quantity induce the change in the factor by the same fraction. The important thing is that the factor could not be parametrized over a

single parameter, background XS of a fuel, because there were different set of SPH factors for the same background XS and there's no theoretical background for it either. The rationale that the parameters were chosen from the property of a pin-cell is that the environmental effect of composition change at other pins on the spectra difference over angle inside a fuel at a pin of interest would be secondary.

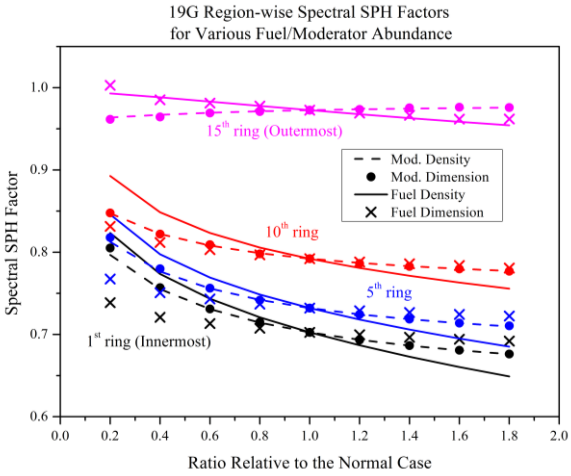

Fig. 10. Region-wise SPH factor behavior according to the change of density and volume of fuel and moderator in 19G. Normal Case = 3w/o UO2 at OPR1000 pin-cell geometry with 500K moderator density (0.843 g/cm^3).

As a means to incorporate resonance interference effect on total XS, a correction factor was separately defined for each resonance isotope other than U238 and used in the similar way as the RIF library method [8] as:

$$\mu_g^{mix}(r) = \mu_g^{U238}(r) + \sum_{iso}\left(f_g^{iso}(r) - 1\right)\mu_g^{U238}(r) \tag{20}$$

The interference correction factor for each isotope is defined as:

$$f_g^{iso}(r) = \frac{\mu_g^{U238+iso}(r)}{\mu_g^{U238}(r)} \tag{21}$$

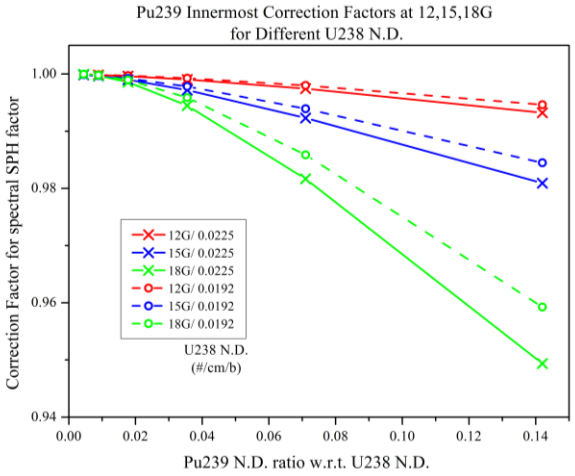

Fig. 11. Innermost Correction Factor behavior of Pu239 for different U238 N.D. at 12,15 and 18G

These correction factors should be tabulated for every case of U238 only case, because even the same number density ratio of a certain isotope with respect to U238 has different correction factors for different absolute number density of U238 as shown in Fig. 11.

These spectral SPH factors together with the correction factors for major resonance isotopes were tabulated over parameters given by Table IV, and evaluated by a region-wise 5-fold linear interpolation in the usage phase. These factors at 1, 2, 3, 5, 10 and 15 rings cases with both the normal and transport corrected ones were tabulated with a single precision in a binary file of 100Mbytes, which is not formidably big to handle.

Table IV. Parameters used for tabulation

Base spectral SPH factor parameters			
Fuel Temperature (K)	300, 600, 900, 1400, 2000		
U238 N.D. (#/cm/b)	0.017, 0.020, 0.023		
Pellet Rad. (cm)	0.37, 0.43, 0.53		
Mod. Src. (#/s)	0.438, 0.766, 1.095[a], 1.423, 1.751		
N.D. ratio of major isotopes w.r.t. U238 N.D.			
U-235	0.001	Cs-133	0.005
Np-237	0.001	Xe-131	0.002
Pu-238	0.005, 0.01	Xe-135	0.000001
Pu-239	0.0125, 0.025, 0.05, 0.1, 0.2	Sm-151	0.0001
		Sm-149	0.0005
Pu-240	0.00625, 0.0125, 0.025, 0.05, 0.1	Eu-154	0.0002
		Eu-155	0.00005
Pu-241	0.003125, 0.00625, 0.0125, 0.025, 0.05	Gd-152	0.0002, 0.0004
		Gd-154	0.002, 0.004
Pu-242	0.01, 0.02	Gd-155	0.02, 0.04
Am-241	0.005, 0.01	Gd-156	0.02, 0.04
Am-243	0.0025, 0.005	Gd-157	0.02, 0.04
Nd-143	0.004	Gd-158	0.02, 0.04
Rh-103	0.002	Gd-160	0.02, 0.04

a : $\Sigma_{mod}V_{mod}$ in 0.876 cm^3 at 500K

IV. PERFORMANCE EXAMINATION

1. Pin-cell Tests

The parametrized spectral SPH factor library method was verified first with the basic pin-cell problems given in Table V. Test types, G, D and T, were for the basic interpolation test with a typical UO2 fuel pin, C was to check the composition effect, and N was to examine non-uniform intra-pellet distribution of number density and temperature cases. The nTRACER calculations were done with McCARD MG XSs at all regions, 15 subrings in a fuel, and 0.01/32/4 ray tracing parameters with P0 scattering treatment. Because this test was for verifying the justification of the parametrization, all the other factors, such as different number of subrings in a fuel and transport correction, were avoided.

Fig. 12 which shows the RMS errors of the interpolated SPH factors from the SPH factor library indicates the soundness of the factor parametrization and interpolation scheme. The interpolated SPH factors were compared with the exact ones generated at the problem of interest. The comparison of the blue and red bars shows the effectiveness of the interference correction factor in Eq. (21), especially for the heavy resonance interference cases, C2 and C5. For ND1 and NT1, the black one used pellet averaged U238 number density or temperature for the SPH factor interpolation, and the green one used region-wise quantities. Although the green ones gave almost the same accuracy with the black ones, the green one is desirable. This will be explained later.

Table V. Pin-cell test problems

Test Type	Test ID	Pellet Radius /Pitch (cm)	Density (g/cm^3) Fuel/Mod	Temperature (K) Fuel/Mod	Composition
G*	G1	0.39/1.27	10.53/0.663	900/600	3w/o UO2
	G2	0.515/1.50	10.53/0.663	900/600	3w/o UO2
D*	D1	0.41/1.26	9.0/0.663	600/600	3w/o UO2
	D2	0.41/1.26	9.0/1.008	300/300	3w/o UO2
T*	T1	0.41/1.26	10.53/0.663	500/500	3w/o UO2
	T2	0.41/1.26	10.53/0.663	700/600	3w/o UO2
	T3	0.41/1.26	10.53/0.663	1200/600	3w/o UO2
C*	C1	0.41/1.27	10.53/0.663	600/600	4.9w/o UO2
	C2	0.41/1.27	9.93/0.663	600/600	14.12% Gd2O3, 2w/o UO2
	C3	0.41/1.27	10.53/0.663	600/600	IFBA 3w/o UO2
	C4	0.41/1.27	10.53/0.663	600/600	1300ppm Boron 3w/o UO2
	C5	0.41/1.27	10.42/0.663	600/600	15% MOX
	C6	0.41/1.27	10.25/0.663	600/600	Burned UO2 (60GWD/MTU) with uniform intra-pellet composition
N*	ND1	0.41/1.26	10.25/0,663	900/600	C6 with real intra-pellet composition
	NT1	0.41/1.26	10.53/0.711	Avg.1316	HFP 200%
				/580	Power Cond. 3w/o UO2

*G: Geometry, D: Density, T: Temperature, C: Composition, N: Non-uniformity

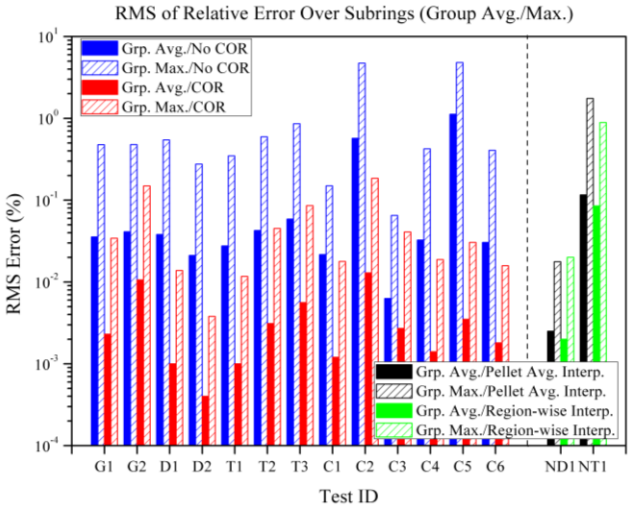

Fig. 12. RMS errors of interpolated SPH factors from the SPH factor library for the tests in Table V

Table VI shows the reactivity error comparison. The reactivity errors due to absorption and nu-fission in a group are evaluated by following and specified for the whole resonance groups respectively.

$$\textbf{Abs.}: \left(\Sigma_{a,g,k}\phi_{g,k}^{(n)}V_k\right)^{ref} - \left(\Sigma_{a,g,k}\phi_{g,k}^{(n)}V_k\right)' \qquad (22)$$

$$\textbf{NuF.}: \frac{1}{k^{ref}} \frac{1}{1+\frac{1}{\left(\nu\Sigma_{f,g,k}\phi_{g,k}^{(n)}V_k\right)' - \left(\nu\Sigma_{f,g,k}\phi_{g,k}^{(n)}V_k\right)^{ref}}}$$

, where $\phi_{g,k}^{(n)}$ is the normalized flux at the region, k, of the group, g, which gives one total fission source in a given problem. In all cases, resonance reactivity errors are greatly reduced and the reason is the restoration of the proper spatial self-shielding of flux as shown in Fig. 6. This improvement is also shown in the right down side of Fig. 13 to 16 with fuel region averaged spectrum errors. The detailed error analysis was done for the problems C1 to C6. Because resonance reaction rate change is inter-connected with the one in thermal groups, group-wise reactivity error changes in entire groups are shown in Fig. 13 to 16, in which 'COR' means the interference correction factor.

C1, the high enrichment UO2 fuel pin, is the one which shows the effectiveness of the proposed method most clearly. No difference between the results with and without the interference correction factor indicates that resonance interference effect of U235 is unimportant.

For C2, the Gadolinia pin, the net reactivity prediction seems to be worse with the spectral SPH factor, but the investigation on group-wise reactivity errors in Fig. 14 reveals that the error in the thermal group is not compensated by the error in the resonance group any more.

The net reactivity error of C5, the heavy MOX fuel pin, is also not that improved much for the same reason of the

C2 case. Unlike the UO2 fuel pin, reactivity errors from nu-fission is similar level to those from absorption in Fig. 16 because of Plutonium isotopes, which results in net small reactivity error from the first.

There are two important observations in both C2 and C5: the need for the correction factor and the restoration of spectrum in both resonance and thermal groups. The ignorance of MG angle dependency let flux in a fuel higher and that in a moderator region smaller, as observed in Fig. 4 and 6, which leads to underestimation of down-scattering neutrons to thermal groups. The lift of thermal spectrum up to the normal level is clearly seen in Fig. 14 and 16.

C3, IFBA, shows not completely improved reactivity error, -560 pcm, which, in fact, comes from thermal groups at IFBA region. Very sharp flux dip at IFBA region cannot be properly simulated that nTRACER IFBA flux is always overestimated at thermal groups, where direct -500 pcm of negative bias is induced. More importantly, higher thermal absorption makes overall lift of fast spectrum and this is why reactivity errors at resonance groups are still high in Table VI. But the point is that the existence of IFBA doesn't harm the accuracy of proper spatial self-shielding of flux.

The 1300 ppm boron case, C4, shows the similar reactivity error improvement except that small negative reactivity error about -20 ~ -30 pcm occurs because the restoration of thermal flux induces slightly higher absorption by boron. The figure is not presented in this paper because it is very similar to Fig. 13.

Table VI. Pin-cell test reactivity results with McCARD MG XS

Test ID	Mc-CARD	nTRACER (McCARD XS)											
		NO SPH				SPH (No Correction Factor)				SPH (Correction Factor)			
	K-eff	K-eff	Δρ (pcm)	Resonance Δρ (pcm)		K-eff	Δρ (pcm)	Resonance Δρ (pcm)		K-eff	Δρ (pcm)	Resonance Δρ (pcm)	
				Abs.	NuF.			Abs.	NuF.			Abs.	NuF.
G1	1.33467	1.32998	-264	-314	+76	1.33465	-1	+9	-3	1.33473	+3	+15	-5
G2	1.26515	1.26030	-304	-379	+114	1.26528	+8	+15	-4	1.26542	+17	+27	-9
D1	1.32780	1.32357	-241	-291	+70	1.32781	+1	+6	-2	1.32794	+8	+13	-4
D2	1.39907	1.39572	-172	-206	+41	1.39921	+7	+10	-4	1.39930	+12	+16	-6
T1	1.35840	1.35420	-228	-272	+66	1.35841	+1	+10	-3	1.35851	+6	+17	-5
T2	1.30692	1.30233	-270	-328	+87	1.30690	-1	+4	-1	1.30700	+5	+12	-6
T3	1.28999	1.28493	-305	-373	+100	1.28997	-1	+4	-1	1.29007	+5	+12	-4
C1	1.40136	1.39686	-230	-299	+106	1.40141	+3	+13	-2	1.40139	+2	+14	-4
C2	0.21050	0.21056	+135	-1558	+1050	0.21037	-294	-353	+251	0.21029	-474	+65	-56
C3	0.81702	0.81141	-846	-620	+280	0.81332	-557	-140	+84	0.81330	-560	-142	+82
C4	1.17986	1.17572	-298	-356	+103	1.17947	-28	-6	+2	1.17955	-22	+3	-2
C5	1.20810	1.20725	-58	-308	+228	1.20832	+15	-62	+60	1.20844	+23	+54	-47
C6	0.93750	0.93443	-350	-413	+95	0.93740	-11	+11	-3	0.93752	+2	+30	-10
		NO SPH				SPH (Average)				SPH (Region-wise)			
ND1	0.92029	0.91714	-373	-449	+95	0.92049	+24	+42	-13	0.92047	+21	+38	-12
NT1	1.30128	1.29608	-308	-367	+93	1.30156	+17	+32	-8	1.30158	+18	+35	-9

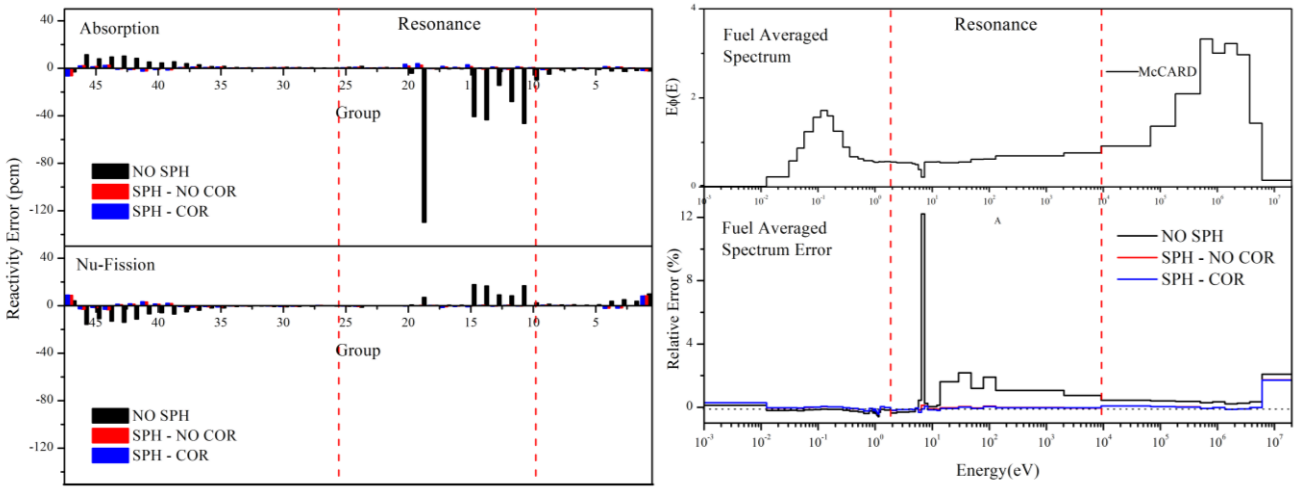

Fig. 13. [Test ID : C1 (Left/Up) Group-wise reactivity error by absorption in a fuel/ (Left/Down) Group-wise reactivity error by nu-fission in a fuel/ (Right/Up) Flue averaged spectrum/ (Right/Down) Fuel averaged spectrum relative error

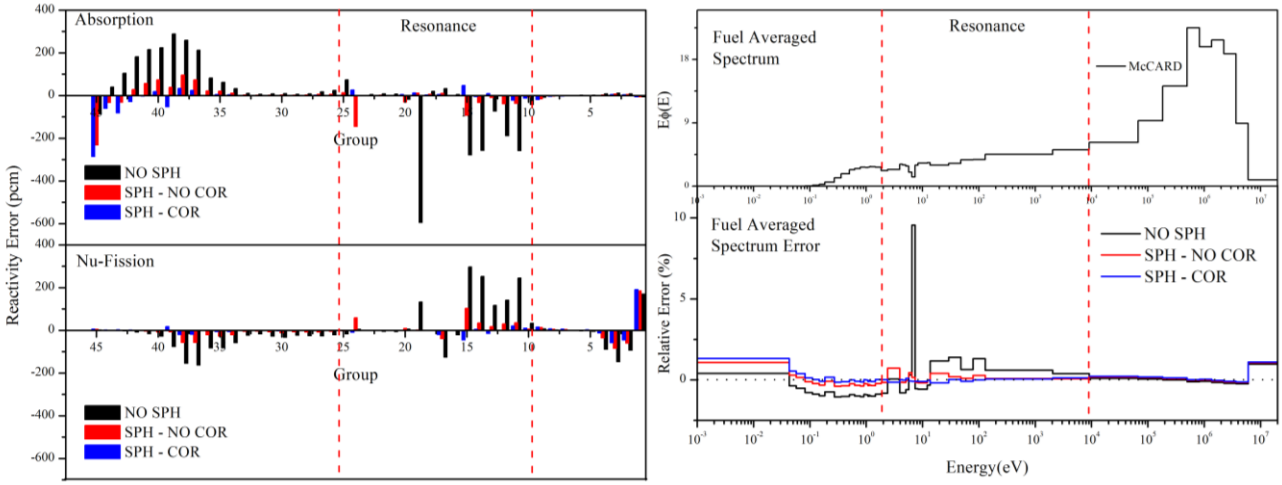

Fig. 14. [Test ID : C2] (Left/Up) Group-wise reactivity error by absorption in a fuel/ (Left/Down) Group-wise reactivity error by nu-fission in a fuel/ (Right/Up) Flue averaged spectrum/ (Right/Down) Fuel averaged spectrum relative error

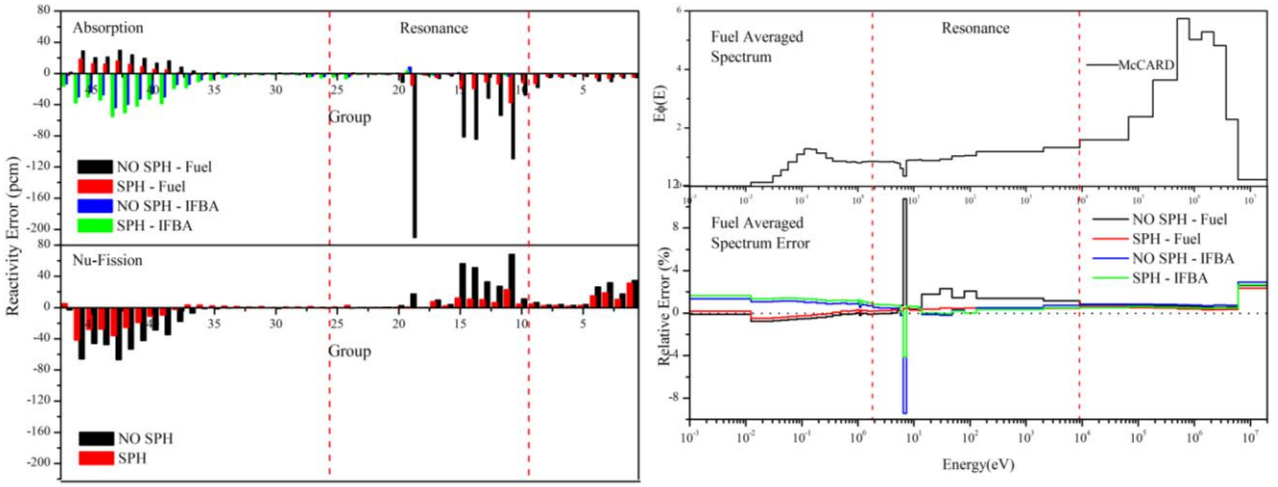

Fig. 15. [Test ID : C3] (Left/Up) Group-wise reactivity error by absorption in a fuel & IFBA/ (Left/Down) Group-wise reactivity error by nu-fission in a fuel/ (Right/Up) Flue averaged spectrum/ (Right/Down) Fuel averaged & IFBA spectrum relative error

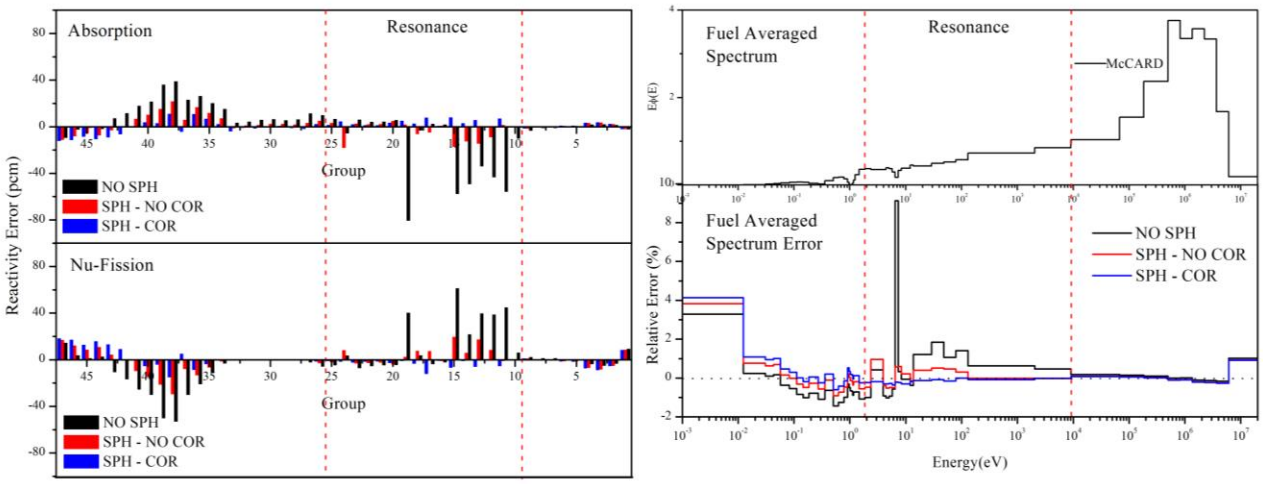

Fig. 16. [Test ID : C5] (Left/Up) Group-wise reactivity error by absorption in a fuel/ (Left/Down) Group-wise reactivity error by nu-fission in a fuel/ (Right/Up) Flue averaged spectrum/ (Right/Down) Fuel averaged spectrum relative error

For the 60GWD/MTU burned fuel with uniform intra-pellet composition, C6, plutonium isotope inventory is much weaker than the C5 case so that the interference correction factor effect is not clearly seen in Table VI. Because spectrum error at resonance groups cannot be perfectly vanished because of its connection with other groups, reactivity errors at resonance groups remain relatively larger than other cases as with the C5 case.

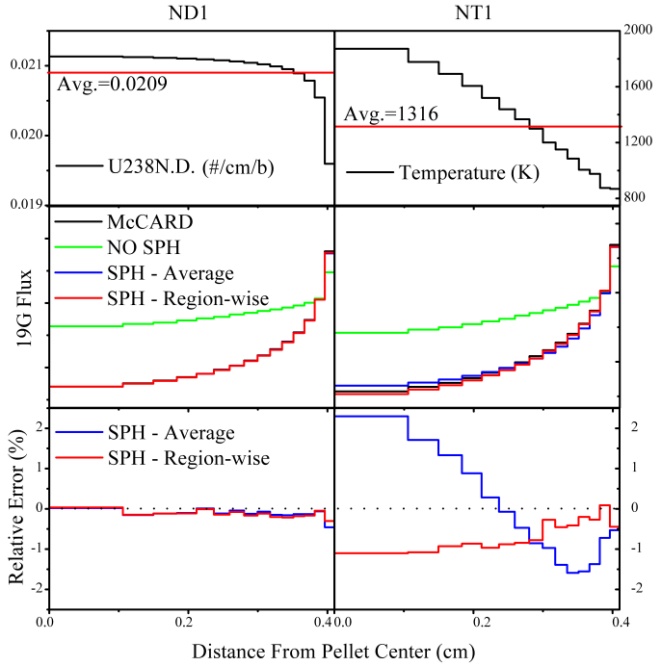

Fig. 17. (Left/Top) [Test ID : ND1] Intra-pellet U238 number density distribution/ (Right/Top) [Test ID : NT1] Intra-pellet temperature distribution/ (Middle) Intra-pellet flux distribution/ (Bottom) Intra-pellet flux relative error

For non-uniform intra-pellet parameter cases, ND1 and NT1, there is an issue whether the region-wise factor should be interpolated by its regional parameter or fuel averaged one. For ND1, the real burn-up U238 number density profile at 60GWD/MTU, the two schemes give no actual difference. For NT1, 200% power level condition at HFP, the interpolation from the regional temperature gives better flux distribution in a view of consistent error behavior. The interpolation from the average temperature makes obvious trend in flux distribution error, low at the periphery and high at the center, which is not desirable in evaluating fuel temperature coefficient. In conclusion, although neither of the two schemes are correct in the strict sense, region-wise spectral SPH factor can be interpolated by using regional parameters.

Lastly, the effectiveness of the new method was compared with the original method, even though the original isotopewise SPH factor method or old SPH method [4] was not intended to resolve the angle dependency of resonance MG XS. Since the old method is only available in the framework of resonance treatment, the new method also used subgroup XS in resonance groups for the equal comparison. Reactivity error improvements of the old SPH method are clearly below the level that the new SPH method has in Table VII. The final big reactivity errors of the new method come from the subgroup method, and thus, such error is not handled in the scope of this paper. The old method cannot recover the flux self-shielding error as exactly as the new method as shown in Fig. 18.

Table VII. Pin-cell test reactivity results with Subgroup XS

Test ID	Mc-CARD	nTRACER (Subgroup XS for resonance groups/ McCARD XS for fast and thermal groups)											
		NO SPH				OLD SPH				NEW SPH			
	K-eff	K-eff	Δρ (pcm)	Resonance Δρ (pcm)		K-eff	Δρ (pcm)	Resonance Δρ (pcm)		K-eff	Δρ (pcm)	Resonance Δρ (pcm)	
				Abs.	NuF.			Abs.	NuF.			Abs.	NuF.
C1	1.40136	1.39565	-292	-364	+111	1.39758	-193	-239	+76	1.40043	-47	-38	+1
C2	0.21050	0.21082	+721	+160	+866	0.21080	+676	+728	+606	0.21057	+158	+1905	-263
C3	0.81702	0.81162	-814	-378	+161	0.81247	-685	-400	+221	0.81364	-508	-90	+84
C4	1.17986	1.17562	-306	-364	+105	1.17734	-181	-213	+69	1.17963	-17	+7	0
C5	1.20810	1.20480	-227	-936	+663	1.20523	-197	-834	+593	1.20625	-127	-555	+389
C6	0.93750	0.92981	-882	-1294	+562	0.93115	-727	-1104	+522	0.93295	-520	-839	+455

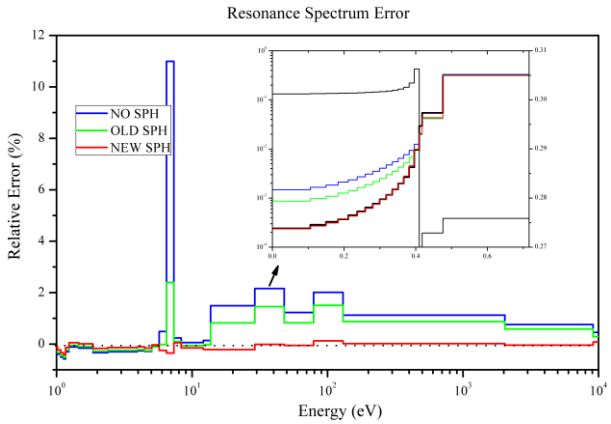

Fig. 18. Resonance spectrum error of the old and new SPH method in C1

Since the isotopewise reaction rate denoted by the numerator in Eq. (23) is not the true one in the effective XS conservation scheme [9] and even in the RI conservation scheme [10] for generating subgroup parameters, the exact reaction rate cannot be preserved even in the pellet averaged sense.

$$\bar{\sigma}_{\rho,g} = \frac{\langle \sigma_\rho \phi \rangle_g}{\langle \phi \rangle_g} = \frac{\sum_n \{\omega_{\rho,g,n}\sigma_{\rho,g,n}\sigma_{b,g,n}/(\sigma_{a,g,n}+\sigma_{b,g,n})\}}{\sum_n \{\omega_{\rho,g,n}\sigma_{b,g,n}/(\sigma_{a,g,n}+\sigma_{b,g,n})\}} \quad (23)$$

As well as the accuracy, the advantage of the new method over the old method is its fast speed because SPH iteration is not needed in the transport calculation. Also, the new method does not belong to any specific resonance treatment so that it can be applied to any transport solver.

2. Assembly Tests

In this section, the new method was verified with a few assemblies. Since the origin of under-estimation of spatial flux self-shielding is the difference of spectra for rays coming into and out of a fuel region, the proposed method will certainly have inter-pin effect as the effective XS does. For example, if there is a water hole instead of a fuel at a neighboring pin, the bigger difference of spectra will cause larger discrepancy of self-shielding. This section is to consider the extent of such a surrounding effect. Three 17 by 17 assemblies were tested as in Fig. 19: A1) HFP UO2 F.A. (VERA 2C), A2) 24 Gadolinia F.A. (VERA 2P) [11], and A3) MOX F.A with the same geometry. The calculation condition was as follow: 0.01 ray spacing, 32 azimuthal angles in a quadrant, 4 optimum polar angles, 5 subrings in a fuel for outflow transport corrected P0 to P3 with McCARD XSs at all regions. For P0 calculation, transport corrected SPH library was used, and for P1 to P3, normal SPH library was used. The implementation result for P1 to P3 is in the reference paper [12]. For region-wise XSs and pin power tally, McCARD used million particles per cycle, 500 inactive and 5,000 active cycles in an octant symmetry.

The result for A1 is shown in Table VIII. The reactivity errors from resonance groups as well as thermal ones are remarkably improved as in the pin-cell test. The reason of the reactivity error improvement in thermal groups is understood from the pin-cell test, C1. In Fig. 13, the initial underestimation of thermal spectrum due to the overestimation of resonance absorption, which causes less absorption and nu-fission in thermal groups, is restored to the normal level. The absolute reactivity error from resonance absorption is somewhat larger for P1 than other cases, but this is considered to be from scattering anisotropy treatment because the error without SPH factor has the same tendency. The pin-power distribution with the new method does not change because the thermal spectrum change is globally affected.

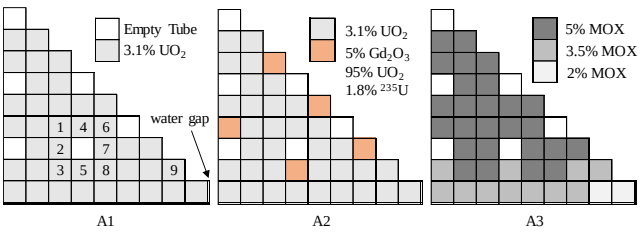

Fig. 19. Assembly test configurations

The pin-wise reactivity error improvement of the P3 result is shown in Fig. 20. Resonance reaction rates are

obviously normalized. The important observation from the resonance reactivity error distribution comparison is that there is no noticeable bias from pins near empty guide tubes.

Table VIII. Assembly A1 (UO2 F.A.) result

Test ID	Method		K-eff	Total Δρ(pcm)	Thermal Δρ		Resonance Δρ		Fast Δρ		Pin Power Diff. (%)	
					Abs.	NuF.	Abs.	NuF.	Abs.	NuF.	RMS	MAX
A1	McCARD		1.17408	1(S.D.)	-	-	-	-	-	-	±0.006	±0.009
	P3	NOSPH	1.17024	-279	125	-138	-382	104	-22	35	0.04	0.07
		SPH	1.17417	7	25	-15	-16	5	-2	9	0.04	0.07
	P2	NOSPH	1.17006	-293	104	-120	-383	105	-14	16	0.05	0.09
		SPH	1.17398	-7	4	3	-17	6	6	-9	0.05	0.09
	P1	NOSPH	1.16979	-312	124	-132	-425	119	-12	13	0.05	0.11
		SPH	1.17373	-25	24	-8	-57	20	7	-12	0.05	0.11
	P0	NOSPH	1.17018	-284	71	-122	-333	94	-22	28	0.05	0.12
		SPH	1.17340	-49	-17	-13	-26	6	-6	8	0.05	0.12

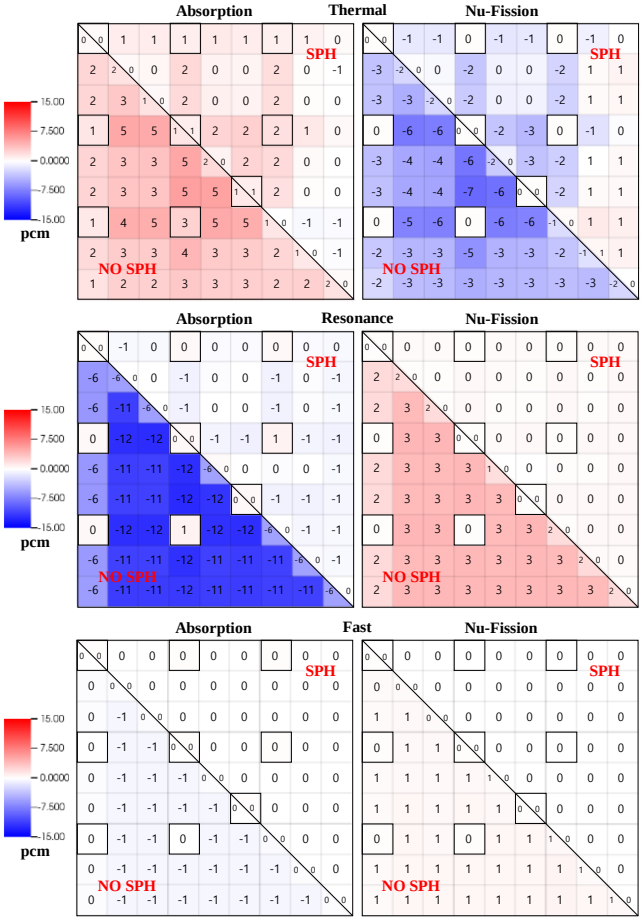

Fig. 20. Comparison of pin-wise reactivity error distribution of thermal, resonance, fast groups with and without spectral SPH factor in the test, A1, with P3 calculation

In fact, there is an effect of more moderators to the spatial flux self-shielding at pins near empty guide tubes, that larger difference of spectra for rays coming into and out of a fuel region makes overestimation of flux in a fuel bigger. This is observed in Fig. 21 that spatial flux self-shielding is more underestimated at the pins, 2,4,5,6,7, which are very next to an empty guide tube, than at the pins, 1,3,8,9. Such difference between the pins, 1,3,8, and the pin, 9 is also observed, but is very small. This difference caused by the abundance of moderator near a pin of interest, the moderator surrounding effect, gives negligible effect on total reactivity improvement. The quantification can be done with Fig. 21 that only about 2% out of 20% flux error improvement is attributed to the moderator surrounding effect. Considering there are 100 pins next to the empty guide tubes, which take up 40% out of total number of fuel pins, the moderator surrounding effect only occupies about 4% of the total reactivity error improvement by the new method. If 300 pcm is improved by only the local effect, about 10 pcm is expected to be more improved by considering the moderator surrounding effect, which is negligible. This was actually tested by considering more moderators for SPH interpolation at pins next to the empty guide tubes to make their fuel averaged flux errors similar to those at other pins, and about 10 pcm improvement was observed.

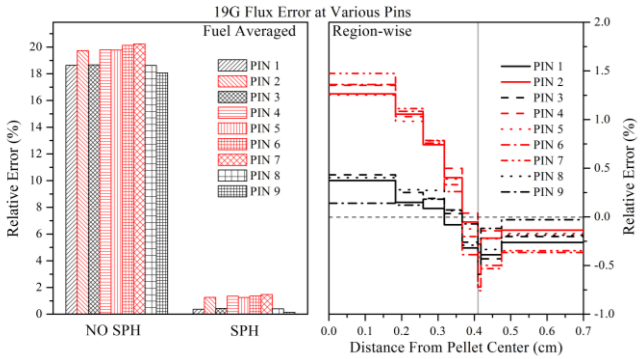

Fig. 21. 19G flux error in a fuel region at pins of locations, 1 to 9 in Fig. 19

The surrounding effect caused by fuel abundance difference or different resonance structure by different resonance isotopes is expected to have much smaller impact than that by moderator abundance difference. Table IX and Fig. 22, 23, the results of A2 and A3, reveal the unnecessariness of the fuel environmental effect, too. Firstly, in Fig 22 and 23, there's no observable difference in

pin-wise resonance reactivity errors among pins near or far from gad pins or different enrichments of MOX fuel. Secondly, exclusion of the moderator surrounding effect doesn't leave any need for further improvement in

Table IX. Assembly A2 (Gadolinia F.A.) and A3 (MOX F.A.) result

Test ID	Method		K-eff	Total Δρ(pcm)	Thermal Δρ		Resonance Δρ		Fast Δρ		Pin Power Diff. (%)	
					Abs.	NuF.	Abs.	NuF.	Abs.	NuF.	RMS	MAX
A2	McCARD		0.91987	1(S.D.)	-	-	-	-	-	-	±0.006	±0.009
	P3	NOSPH	0.91652	-397	139	-225	-506	167	-30	58	0.07	0.14
		SPH	0.91932	-65	-18	-39	-39	18	-7	21	0.09	0.21
	P2	NOSPH	0.91670	-376	146	-222	-492	162	-29	60	0.07	0.15
		SPH	0.91950	-44	-10	-36	-26	13	-7	23	0.09	0.23
	P1	NOSPH	0.91567	-499	112	-263	-578	197	-33	65	0.07	0.15
		SPH	0.91847	-166	-46	-76	-108	48	-11	28	0.08	0.15
	P0	NOSPH	0.91825	-192	209	-160	-380	124	-20	36	0.16	0.36
		SPH	0.92053	78	71	4	10	-10	-2	6	0.17	0.34
A3	McCARD		1.08534	1(S.D.)	-	-	-	-	-	-	±0.006	±0.009
	P3	NOSPH	1.08195	-289	168	-216	-437	182	-20	34	0.07	0.16
		SPH	1.08499	-30	0	-18	-30	15	0	3	0.08	0.16
	P2	NOSPH	1.08212	-274	170	-211	-425	176	-19	35	0.07	0.16
		SPH	1.08516	-15	3	-14	-19	10	0	4	0.08	0.17
	P1	NOSPH	1.08110	-361	171	-263	-511	224	-22	39	0.08	0.20
		SPH	1.08415	-101	2	-64	-101	57	-2	7	0.09	0.20
	P0	NOSPH	1.08327	-176	168	-158	-328	132	-16	25	0.16	0.35
		SPH	1.08460	-63	-45	-4	-8	-12	-9	16	0.16	0.36

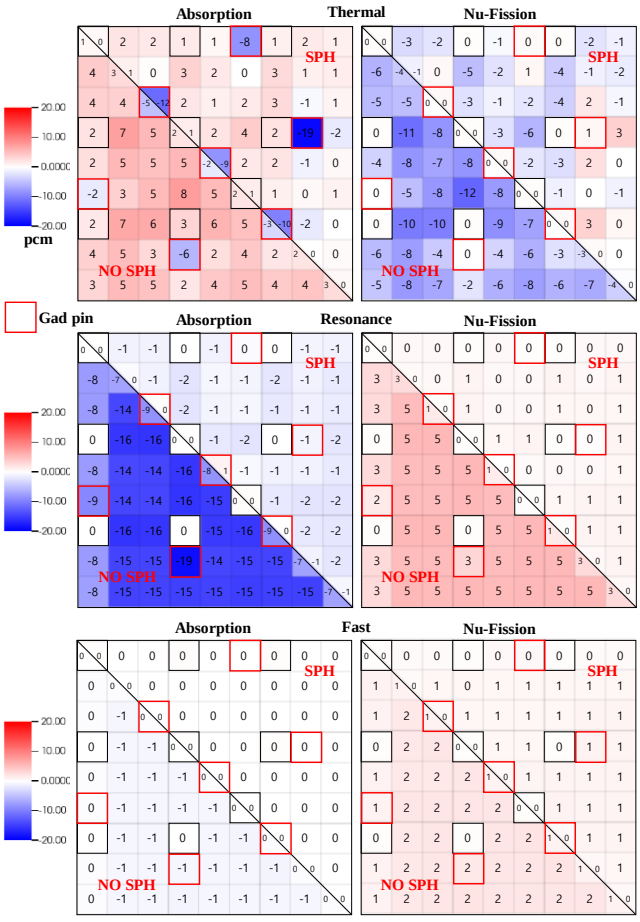

Fig. 22. Comparison of pin-wise reactivity error distribution of thermal, resonance, fast groups with and without spectral SPH factor in the test, A2, with P3 calculation

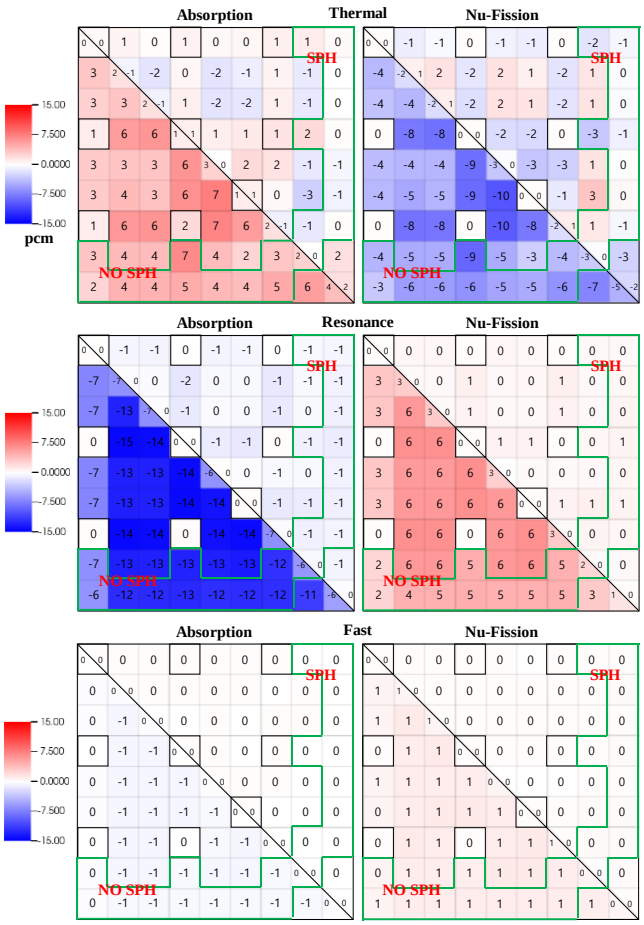

Fig. 23. Comparison of pin-wise reactivity error distribution of thermal, resonance, fast groups with and without spectral SPH factor in the test, A3, with P3 calculation

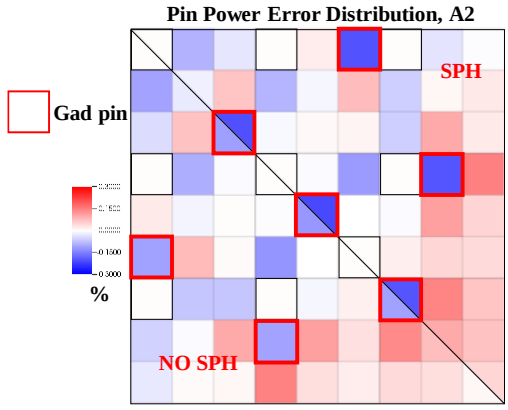

Fig. 24. Comparison of pin power error distribution with and without spectral SPH factor in the test, A2, with P3 calculation

resonance reactivity error in Table IX because small non-negligible remaining error also exists in the C2 and C5 case of the pin-cell test.

One thing to note in A2 is that the higher maximum pin-power error comes from among gad pins. The initially lower power in gad pins in Fig. 24 is caused by the underestimation of thermal flux in a gad pin as shown in Fig. 14. Considering the same increase ratio of thermal flux and absolute smaller value of power in gad pins compared to those in normal fuel pins, pin power at gad pins becomes relatively smaller after the SPH correction. That is why the pin power errors in gad pins are more negative. This example indicates the possibility of pin power error aggravation with this method when the actual MG library is used for a shimmed assembly due to the thermal flux elevation after the SPH correction.

V. CONCLUSIONS

This paper demonstrates the mechanism by that the ignorance of the resonance MG XS angle dependency causes severe over-estimation of intra-pellet flux, which leads to large negative reactivity bias regardless of group structure. This problem could be resolved by introducing the region-wise spectral SPH factor to the approximated transport operator in a transport calculation.

The generalization of the spectral SPH factor was done with its successful parametrization over fuel radius, U238 number density, moderator source and square root of temperature within less than 0.1% error. In addition, the interference correction factor plays an important role in yielding accurate enough flux self-shielding for heavy resonance interference cases.

The miscellaneous considerations for the application to an actual transport calculation were also tested. It was shown that direct interpolation was enough for the space interpolation of the factor with the exact value tabulation of 15,10,5,3,2,1 rings cases. Transport corrected SPH iteration was used for transport corrected P0 transport calculation and normal SPH iteration was used for PN calculation.

The consequence of the new method was examined by various pin-cell cases. The imbalance of flux error, higher in resonance and smaller in thermal groups, was recovered by the application of SPH factor only to resonance groups, by which -200 ~ -300 reactivity bias almost vanished. The new method was turned out to be superior to the old method whose performance was less than half of the new one. For a real burned fuel, region-wise parameter interpolation was accurate enough. For non-uniform intra-pellet temperature cases, it was shown that region-wise parameter interpolation was better than the pellet averaged parameter interpolation. However, it should be examined more closely in evaluating fuel temperature coefficient in connection with resonance treatment in a further research.

The new method was also proved to be effect in the assembly calculations. It turned out that the surrounding effect took only about 4% of the reactivity improvement of the new method, thus considering the local effect is enough. However, due to the elevation of thermal flux, there can be an aggravation of pin power distribution for shimmed

assembly. In this sense, further research about handling thermal flux error should follow.

With the proposed method, about -200 to -300 pcm of hidden reactivity bias was resolved. As a result, other error factors which have remarkably been balanced well with the hidden bias will emerge. Such errors should be identified and fixed for high fidelity reactor simulations in the future research.

ACKNOWLEDGMENTS

This work was supported by the Ministry of Science, ICT and Future Planning of Korea through National Research Foundation of Korea (NRF) Grant 2014M2A8A2074094.

REFERENCES

1. G. I. BELL, G. E. HANSEN, and H. A. SANDMEIER, "Multitable Treatments of Anisotropic Scattering in S_N Multigroup Transport Calculation," *Nucl. Sci. Eng.*, **28**, 376 (1967).
2. A. GIBSON, "Novel Resonance Self-Shielding Methods for Nuclear Reactor Analysis," MIT, Cambridge (2016).
3. A. HEBERT, "A Consistent Technique for the Pin-by-Pin Homogenization of a Pressurized Water Reactor Assembly," *Nucl. Sci. Eng.*, **113**, 227 (1993).
4. A. HEBERT, "Advances in the Development of a Sub-group Method for the Self-Shielding of Resonant Isotopes in Arbitrary Geometries," *Nucl. Sci. Eng.*, **126**, 245 (1997).
5. Y. S. JUNG, H. G. JOO and et al., "Practical Numerical Reactor Employing Direct Whole Cole Neutron Transport and Subchannel Thermal/Hydraulic Solvers," *Ann. Nucl. Energy*, **62**, 357 (2013).
6. H. J. SHIM, B. S. HAN and et al., "McCARD : Monte Carlo Code for Advanced Reactor Design and Analysis," *Nucl. Eng. Technol.*, **44**, 161 (2012).
7. A. YAMAMOTO, Y. KITAMURA, and Y.YAMANE, "Simplified Treatments of Anisotropic Scattering in LWR Core Calculations," *J. Nucl. Sci. Technol.*, **45**, 217 (2008)
8. S. Y. CHOI, D. J. LEE and et al., "Resonance Self-shielding Method using Resonance Interference Factor Library for Practical Lattice Physics Computations of LWRs," *J. Nucl. Sci. Technol.*, **53**, 1142 (2016)
9. H. G. JOO, L. POGOSBEKYAN and et al., "Subgroup Weight Generation Based on Shielded Pin-cell Cross Section Conservation," *Ann. Nucl. Energy*, **36**, 859 (2009)
10. R. J. STAMML'ER, and et al., "HELIOS Methods." Studsvik Scandpower (2003)
11. A. T. Godfrey, "VERA Core Physics Benchmark Progression Problem Specifications," Revision 3, CASL-U2012-0131-003, CASL (2014)
12. M. Ryu, H. G. JOO and et al., "Incorporation of Anisotropic Scattering in nTRACER," *Trans. KNS Autumn Meeting*, Oct 30-31 (2014)